Why the Properties of El Niño Changed During the Late 1970s

Bin Wang and Soon-Il An

School of Ocean and Earth Science and Technology, University of Hawaii at Mãnoa, Honolulu, HI 96822

Abstract. Following the abrupt North Pacific climate shift in the mid-1970s, the period, amplitude, spatial structure, and temporal evolution of the El Niño notably changed. Theory is needed to explain why the coherent changes in several El Niño characteristics are nearly synchronized with the decadal climate shift. While the decadal variation in the equatorial thermocline could potentially change El Nino behavior, observation indicates that from the pre-shift (1961 – 1975) to the post-shift (1981 – 1995) period the change of equatorial eastern Pacific thermocline is insignificant. Our numerical experiments with a coupled atmosphere-ocean model illustrate that the observed changes in ENSO properties may be attributed to decadal changes in the surface winds and associated ocean surface layer dynamics without changes in the mean thermocline. A theoretical analysis is presented to elucidate the mechanisms by which the decadal variations in winds and upwelling modify the structure and propagation of the El Niño and amplify and prolong the El Niño-La Niña cycle.

The dominant period of the El Niño increased from 2-3 years during 1960s and 1970s to 4-5 years during 1980s and 1990s; during this time the amplitude of El Niño also increased [*An and Wang*, 2000]. These changes were accompanied by a notable modification in the evolution pattern and spatial structure of the coupled ocean-atmospheric anomalies. During 1960s and 1970s the warm SST anomalies expanded westward from the South American coast into the central equatorial Pacific [*Rasmusson and Carpenter*, 1982]; after 1980, the warm SST anomalies propagated eastward across the basin from the central Pacific or developed concurrently in the central and eastern Pacific [*Wallace et al*., 1998]. A joint singular value decomposition (JSVD) method [*Bretherton et al*., 1992], a tool for depicting coupled patterns among multiple geophysical variables, was used to portray the dominant patterns derived for the 1961-75 and 1981-95 periods, respectively (Fig. 1). The maximum SST gradient, strongest zonal wind stress, and steepest thermocline slopes along the equator were all displaced eastward about 15 degrees longitude during 1981-95.

Fig. 1

The change in ENSO (El Niño and Southern Oscillation) properties was nearly concurrent with a remarkable climate shift in the extratropical Pacific Ocean –an abrupt change in the SST and large-scale winter circulation over the North Pacific observed in the mid-1970s [*Trenberth and Hurrel*, 1994]. Over the tropical Pacific, a corresponding shift occurred in the background state of the coupled atmosphere-ocean system [*Graham*, 1994].

The ENSO is sensitive to changes in the ocean background conditions [*Kleeman et al*., 1999], but how variations in the background state modulate the properties of ENSO remains a subject of debate. *Fedrov and Philander* [2000] emphasized the role of secular changes of thermocline in modulating ENSO behavior. The subtropical SST anomalies can be subducted into the equatorial thermocline, eventually affecting the equatorial SST [*Gu and Philander*, 1997]. On the other hand, *Kleeman et al*. [1999] suggested that the altered heat transport in the *upper branch* of the oceanic subtropical cell conveys the impact of the decadal oscillation originating in midlatitudes to the equatorial SST. Two critical aspects concerning the origin of the decadal variation of ENSO have been overlooked, i.e., the coherent changes of the amplitude, frequency, structure, and evolution of ENSO, and the concurrent occurrence of the extratropical decadal climate shift and the change of El Nino properties. The present paper calls for attention to these issues and offer a new explanation as to why the coherent changes in several El Niño characteristics are nearly synchronized with the decadal climate

shift. We focus on two contrasting 15-year-periods before (1961-1975) and after (1981-1995) the Pacific climate shift, because the available data for these two periods are better than for any other and because the changes in both the background state and ENSO properties are most prominent around the late 1970s.

Observed changes in the background state

The data sets used to detect tropical decadal variations include the Florida State University (FSU) pseudo wind stress [*Shriver and O'Brien*, 1995] and surface winds compiled by da Silva [*da Silva et al*., 1994], the NCEP/NCAR reanalysis SST [*Kalnay et al*., 1996], the Levitus ocean temperature [*Levitus and Boyer*, 1994], and the temperature data assimilated at the University of Maryland by *Carton et al*. [2000] using the Simple Ocean Data Assimilation package (SODA data).

The mean surface winds during the 1981-95 period shows weaker easterlies in the western Pacific and stronger easterlies in the eastern Pacific, with convergence in the central Pacific around (160°W, 7°S) (Fig. 2). These features are commonly seen in both the FSU and da Silva's data sets. The equatorial wind anomalies are associated with trade wind anomalies in both hemispheres, thus they are connected with the extratropics. From 1961-75 to 1981-95, the mean tropical Pacific SST increased, particularly over the equatorial central Pacific and the southeastern tropical Pacific where the rise in SST exceeds 0.5 °C**.** The changes in SST are consistent with the changes in wind stress in that the winds tend to converge into regions of warm SST in the western-central Pacific, and the changes agree with the Matsuno-Gill [*Gill*, 1980] solution for a steady atmospheric response to an enhanced convective heat source caused by a warm SST. This dynamic consistency adds confidence to the described changes in the surface winds and SST.

Fig. 2

The decadal mean equatorial thermocline depths (represented by the 20°C isotherm depth) derived from Levitus data averaged over 4.5°S ~ 4.5°N for the two periods are similar (Fig. 3). Lack of long-term subsurface ocean data makes it difficult to estimate reliably changes in the thermocline. For this reason, we have examined another subsurface temperature data, the SODA data, which shows a rise in the thermocline depth primarily in the western equatorial Pacific after the climate shift. Part of the discrepancies between the Levitus data and the SODA data might arise from the fact that the SODA model is forced by a detrened wind stress field [*Carton et al*., 2000]. Removal of long-term trends may have reduced the magnitude of the decadal variations in surface winds and affected the decadal variations in the thermocline.

Fig. 3

The mean thermocline depth, surface layer currents, and upwelling were computed using the Cane and Zebiak [*Zebiak and Cane*, 1987] ocean model forced by the two 15-year mean climatological annual cycles of the FSU wind stress. The change in thermocline depth is moderate in the eastern equatorial Pacific (Fig. 3). During the 1981-95 period the equatorial mean upwelling increased over the eastern Pacific (160°W-100°W), and decreased over the central Pacific (150°E-160°W). This is a consequence of stronger trade winds over the eastern Pacific and weaker ones over the central Pacific (Fig. 2). Consistent with the change in winds, the equatorial eastward currents increased in the western-central Pacific while reduced in the eastern Pacific.

While a secular change in the background thermocline may change ENSO characteristics, analysis of available observations doesn't show any significant decadal change in thermocline in the equatorial eastern Pacific where the El Niño is most perceptive to the subsurface variability. Pronounced changes in the tropical Pacific background state, however, are found in surface wind and SST fields. The question is: Can the observed changes in the background state of these fields alter the properties of ENSO?

Results of Numerical experiments

Numerical experiments were performed to explore what causes the differences in ENSO properties during the pre- and the post-climate

shift periods. We used the coupled ocean-atmospheric model developed by *Zebiak and Cane* [1987] (CZ model), in which the basic states of the atmosphere and ocean are specified. To avoid model drifts away from the original CZ model, the basic state used for 1961-75 (1981-95) is an average of the observed basic state for 1961-75 (1981-95) and the original CZ model basic state, which includes surface wind, atmospheric divergence, SST, currents, upwelling, thermocline depth, and coefficient relating thermocline fluctuations to the subsurface temperature.

The model ENSO produced using the 1961-75 basic state has a shorter period (about 3 years) and a smaller amplitude (the standard deviation of the Niño-3 SSTA is 0.94°C), and the warm SST anomalies propagate westward (Fig. 4a). In contrast, the ENSO produced using the 1981-95 basic state exhibits a longer period (about 4 years) and a larger amplitude (the standard deviation is 1.32°C), and the warm SST anomalies are stationary or propagate eastward (Fig. 4b). The structures of the dominant ENSO modes appearing under the two background state conditions are depicted using the JSVD analysis of the anomalous SST, zonal wind stress, and thermocline depth fields. As shown in Fig. 5, the spatial patterns of the primary JSVD mode resemble those derived from the observations (Fig. 1): The anomalous westerly patch, the largest zonal gradients of the thermocline depth and SST anomalies are all displaced eastward by about 15 degrees longitudes from the 1961-75 to the 1981-95 period. Thus, the model ENSO characteristics obtained using the two sets of basic-state parameters were qualitatively consistent with their observed counterparts, suggesting that the interdecadal changes in the basic state may cause the observed coherent changes in ENSO.

Fig. 4

To reveal which factors in the background states influence the model ENSO the most, we first assessed the relative contributions of background SST and surface winds (including associated ocean circulation). In a group of experiments, all the basic-state parameters were given the 1961-75 values with the exception that either SST *or* surface wind (and associated oceanic fields) was given its 1981-95 value. When only SST had its 1981-95 value, the model ENSO resembled the one obtained using the 1961-75 basic state values (figure not shown), implying that changing only the background state SST does not significantly influence the model ENSO. On the other hand, when the basic state winds and the associated ocean circulation had their values of the 1981-95 period while the other parameters remained at the 1961-75 values, the model ENSO was similar to the one obtained using the 1981-95 basic state values. These results suggest that changes in the surface winds and associated oceanic conditions are responsible for the changes in the model ENSO. Noted that in the CZ model, atmospheric heating depends on the total SST; thus, when SST and winds are specified independently, the only way for the basic state SST to affect ENSO is through altering convective heating. Thus, the results here imply that the atmospheric heating due to changes in the basic state SST has little effect on the model ENSO behaviour, while changes in background winds and associated ocean circulation play a dominant role.

Fig. 5

Additional experiments were designed in a similar manner to assess the roles of the background thermocline, upwelling, and ocean currents in regulating ENSO when surface winds have the observed decadal shift. It is found that as long as the background surface winds and associated mean upwelling changed from 1961-75 to 1981-95 values, the changes in ENSO behaviour resemble those in the benchmark experiment (Fig. 4) regardless of which decadal values of the background thermocline depths or currents are used. On the other hand, the decadal changes in thermocline alone or in ocean currents alone were not able to reproduce the change in ENSO behaviour shown in Fig. 4. The conclusion holds regardless of which thermocline changes shown in Fig. 3 are used. Therefore, the changes in ENSO properties are mostly attributable to alterations in background winds and associated mean upwelling.

Theoretical interpretation

How do the basic state winds change the spatial and temporal structure of ENSO? The most prominent structural change is an eastward displacement of the equatorial wind anomalies during 1981-95. Our diagnostic analyses identified two processes responsible for this eastward displacement. First, during the 1981-95 period the trade winds became stronger and converged more in the equatorial eastern Pacific (Fig. 2) that favours an eastward extension of the atmospheric heating and associated equatorial westerly anomalies. Secondly, the change in background winds enhanced the mean upwelling in the eastern Pacific while suppressing it in the central Pacific, thus creating zonally differential temperature advection by the mean upwelling and leading to an eastward shift of the maximum zonal SST gradient. By affecting surface buoyancy fluxes, the zonal SST gradients created a zonal pressure gradient force in the atmospheric boundary layer, which promoted an eastward displacement of the equatorial westerly anomalies.

The propagation of SST anomalies is primarily determined by competitive effects between the vertical temperature advection, which promotes eastward propagation and the zonal temperature advection, which induces westward propagation [*Fedorov and Philander*, 2000]. From the pre- to the post-shift periods, the vertical advection plays a more important role than the zonal advection, thus prevailing westward propagation was replaced by stationary or eastward propagation. The decadal changes in the vertical advection can be attributed to the mean thermocline depth change or the mean upwelling change [*An and Jin*, 2000]. *Fedorov and Philander* [2000] stressed the effect of changing the mean thermocline, whereas here we emphasize the effect of changing the mean upwelling.

Why do the ENSO frequency and amplitude change? Using a coupled model, we have illustrated that the period of the model ENSO indeed lengthened when the westerly anomalies were shifted eastward [*An and Wang*, 2000]. We now explain the mechanism using a conceptual model. We first show that an eastward relocation of the westerly anomalies can amplify thermocline fluctuations in the eastern Pacific and across the entire equatorial basin. Let us consider a reduced-gravity shallow-water system with three equatorial boxes representing the western, central, and eastern Pacific. On the ENSO time scale, the zonal pressure gradient force associated with the thermocline tilt approximately balances the equatorial wind stress [*Jin*, 1996], which leads to the following relationship between the thermocline anomaly in the western (h_W) and eastern (h_E) Pacific:

$$h_E - h_W = a_L \tau(t), \quad (1)$$

where $\tau(t)$ represents the zonal wind stress anomaly over the central Pacific and a_L is a parameter establishing the balance between the wind stress and the east-west difference in the thermocline depth. Since the Rossby and Kelvin waves excited by the central Pacific wind stress constantly adjust the thermocline, changes in h_E are not only due to the wind forcing, $a_L\tau(t)$, but also due to the remotely forced Kelvin waves. The westerly wind stress in the central Pacific during a warm phase of ENSO (Fig. 1) produces positive wind stress curl on each side of the equator, which generates upwelling Rossby waves. These westward Rossby waves, upon being reflected at the western boundary, induce upwelling Kelvin waves propagating eastward, which lower the eastern Pacific thermocline. Thus, the reflected Kelvin wave-induced thermocline depth anomaly always lags and opposes the anomaly created directly by the central Pacific wind forcing. Hence, it may be expressed by $-a_w\tau(t-s)$ [*Battisti and Hirst*, 1989], where the coefficient a_w measures the strength of the reflected Kelvin wave and the time lag s represents the time needed for Rossby waves to travel from their forced region to the western boundary plus the reflected Kelvin waves to cross the equatorial basin. Thus, h_E becomes

$$h_E = a_L \tau(t) - a_w \tau(t-s). \quad (2)$$

Here we have omitted the time taken by Kelvin waves to pass through the basin, because they propagate much faster than a package of Rossby waves. From (1) and (2), the zonal mean thermocline depth anomaly ($(h_E+h_W)/2$) becomes:

$$[h] = 0.5\, a_L \tau(t) - a_w \tau(t-s) \quad (3)$$

The time lag, *s*, depends on the longitudinal position of the equatorial westerly anomaly. An eastward shift of the anomalies means an increased time lag. Suppose $\tau(t) = Re\{Fe^{i\omega t}\}$and [h] = $Re\{He^{i\omega t}\}$, where *F* and *H* are amplitudes of the wind stress and [*h*], respectively, for a given oscillation frequency, ω. Then, the amplitudes of the h_E and [*h*] would be proportional to the square root of $a_L^2+a_w^2-2a_La_w\cos(\omega s)$ and $0.25a_L^2+a_w^2-a_La_w\cos(\omega s)$, respectively. Because the time lag *s* cannot exceed one-half the period of the oscillation, an increase in *s* implies an amplification of h_E, and $[h]$[1].

Amplification of the thermocline anomalies in the eastern Pacific, h_E would enhance the growth of an *in-situ* SST anomaly in the eastern Pacific by strengthening the vertical temperature advection [*Philander et al*., 1984]. An increase in zonal mean thermocline depth anomaly, [*h*] would prolong the oscillation period, because the time required to recharge and discharge the water mass in the equatorial region would increase according to the recharge/discharge model of ENSO [*Jin*, 1996].

Discussion

We have demonstrated that the observed changes in ENSO properties may be attributed to decadal changes in the surface winds and associated ocean surface layer dynamics without changes in the mean thermocline. The model results reveal a critical role of the atmospheric teleconnection, which could rapidly convey the impact of extratropical decadal variations to ENSO through changing surface winds and equatorial upwelling. The proposed mechanism is appealing in that it explains the coherent changes in several ENSO characteristics and their concurrent occurrence with the decadal climate shift in the extratropics. Our results suggest that the Pacific climate shift may have altered ENSO properties by changing background tropical winds and associated equatorial upwelling. In view of the simplicity of the model and uncertainty of the observations, our model results are qualitatively indicative. It is hoped that this study will stimulate more comprehensive investigations. Nevertheless, The mechanisms revealed in this study shed light on the decadal variability in ENSO predictability. In view of the threat of global warming, we need to know how increased greenhouse gas concentrations will affect tropical winds, especially the equatorial winds, so that we can assess its potential impacts on El Niño.

[1] When the delay lag s is increased from zero to a quarter cycle of the oscillation period, the thermocline depth anomalies in the eastern Pacific, h_E and the entire equatorial basin, [*h*], are increased by about 26 % and 20 %, respectively. In SODA data, from the pre-shift to the post-shift period the root-mean-square of thermocline depth anomalies in the eastern Pacific (150°W-90°W, 3°S-3°N) and the entire equatorial basin (3°S-3°N) increased about 14% and 11%, respectively.

Acknowledgements. This study is supported by NOAA OGP Pacific Program and by Frontier Research System for Global Chang through its sponsorship of the International Pacific Research Center. The authors appreciate Dr. G. Speidel for editing an earlier version of the manuscript. SOEST contribution 5574 and IPRC contribution IPRC-91.

References

An, S.-I. And F.-F. Jin, An eigen analysis of the interdecadal changes in the structure and frequency of ENSO mode. *Geophys. Res. Lett*., **27**, 2573-2576, 2000.

An, S.-I. and B. Wang, Interdecadal change of the structure of the ENSO mode and its impact on the ENSO frequency. *J. Climate*, **13**, 2044-2055, 2000.

Battisti, S. D. and A. C. Hirst, Interannual variability in the tropical atmosphere-ocean model: Influence of the basic state, ocean geometry, and nonlinearity. *J. Atmos. Sci*., **46**, 1678-1712, 1989.

Bretherton, C., C. Smith, and J. Wallace, An intercomparison of methods for finding coupled patterns in climate data. *J. Climate*, **5**, 541-560, 1992.

Carton, J. A., G. Chepurin, X. Cao, and B. Giese, A simple ocean data assimilation analysis of the global upper ocean 1950-95. Part I: methodology. *J. Phys. Oceanogr*., **30**, 294-309, 2000.

da Silva, A., A. C. Young, and S. Levitus, *Atlas of Surface Marine Data 1994*, NOAA Atlas NESDIS **6**, U.S. Dept. of Commerce, 1994.

Fedorov, A. V. and S. G. H. Philander, Is El Niño changing? *Science*, **228**, 1997-2002, 2000.

Gill, A. E., Some simple solutions for heat-induced tropical circulation *Quart. J. Roy. Meteor. Soc*., **106**, 447-462, 1980.

Graham, N. E., Decadal-scale climate variability in the tropical and North Pacific during the 1970s and 1980s: observations and model results. *Climate Dyn*., **10**, 135-162, 1994.

Gu, D. and S. G. Philander, Interdecadal climate fluctuations that depend on exchange between the tropics and extratropics. *Science*, **275**, 805-807, 1997.

Jin, F.-F., Tropical ocean-atmosphere interaction, the Pacific cold tongue, and the El Niño-Southern Oscillation. *Science*, **274**, 76-78, 1996.

Kalnay, E. and Coauthors, The NCEP/NCAR 40-year reanalysis project. *Bull. Am. Meteorol. Soc*., **77**, 437-471, 1996.

Kleeman, R., J. McCreary, and B. Klinger, A mechanism for generating ENSO decadal variability. *Geophys. Res. Lett*. **26**, 1743-1746, 1999.

Levitus, S. and T. Boyer, *World Ocean Atlas 1994*, NOAA atlas NESDIS **4**, U.S. Department of commerce, Washington, DC, 1994.

Philander, S. G. H., T. Yamagata, and R. C. Pacanowski, Unstable air-sea interactions in the tropics. *J. Atmos. Sci*., **41**, 604-613, 1984.

Rasmusson, E. M. and T. H. Carpenter, Variations in tropical sea surface temperature and surface wind fields associated with the Southern Oscillation/El Niño. *Mon. Wea. Rev*., **110**, 354-384, 1982.

Shriver, J. F. and J. J. O'Brien, Low-frequency variability of the equatorial Pacific ocean using a new pseudostress dataset: 1930-1989. *J. Climate*, **8**, 2762-2786, 1995.

Trenberth, K. E. and J. W. Hurrel, Decadal atmosphere-ocean variations in the Pacific. *Clim. Dyn*., 9, 303-319, 1984.

Wallace, J., E. Rasmusson, T. Mitchell, V. Kousky, E. Sarachik, and H. von Storch, On the structure and evolution of ENSO-related climate variability in the tropical Pacific: lessons. *J. Geophy. Res*., **103**, 14241-14259, 1998.

Zebiak, S. E., and M. A. Cane, A model El Niño-Southern Oscillation. *Mon. Wea. Rev*., **115**, 2262-2278, 1987.

[*]Bin Wang and Soon-Il An, International Pacific Research Center ([*]Dept. of Meteorology), SOEST, University of Hawaii, Honolulu, HI 96822. (e-mail: bwang@soest.hawaii.edu, sian@soest.hawaii.edu)

(Received)

Figure Captions

Fig. 1 The loadings of the principal Joint-SVD mode derived from SODA data for the period of 1961-75: (a) SST (contour intervals: 0.2 ^{o}C), (b) zonal wind stress (contour intervals: 0.5×10^{-3} N m^{-2}), and (c) thermocline depth represented by the 20 ^{o}C isotherm depth (contour intervals: 3 m). The right panels (d), (e), and (f) are the counterparts of the corresponding left panels for the 1981-95 period. The thick solid lines indicate locations of the maximum zonal SST gradients (panel a and d), the maximum equatorial westerly anomalies (panel b and e), and the maximum slope of the thermocline depth anomalies (panel c and f). First JSVD modes for the period of 1961-75 and 1981-95 explain 84.4% and 84.8% of total variance, respectively.

Fig. 1 The loadings of the principal Joint-SVD mode derived from SODA data for the period of 1961-75: (a) SST (contour intervals: 0.2 ^{o}C), (b) zonal wind stress (contour intervals: 0.5×10^{-3} N m^{-2}), and (c) thermocline depth represented by the 20 ^{o}C isotherm depth (contour intervals: 3 m). The right panels (d), (e), and (f) are the counterparts of the corresponding left panels for the 1981-95 period. The thick solid lines indicate locations of the maximum zonal SST gradients (panel a and d), the maximum equatorial westerly anomalies (panel b and e), and the maximum slope of the thermocline depth anomalies (panel c and f). First JSVD modes for the period of 1961-75 and 1981-95 explain 84.4% and 84.8% of total variance, respectively.

Fig. 2 Differences in the annual mean pseudo wind stress (vector) and SST (contour) between the 1961-75 and 1981-95 periods (1981-95 minus 1961-75). The units for SST are °C and the scale for wind stress is given by the arrow located at the upper right corner. The SST and wind stress data are derived from NCEP/NCAR reanalysis SST and from FSU wind stress data, respectively.

Fig. 2 Differences in the annual mean pseudo wind stress (vector) and SST (contour) between the 1961-75 and 1981-95 periods (1981-95 minus 1961-75). The units for SST are °C and the scale for wind stress is given by the arrow located at the upper right corner. The SST and wind stress data are derived from NCEP/NCAR reanalysis SST and from FSU wind stress data, respectively.

Fig. 3 Decadal differences in the mean depth of the 20°C isotherm (the 1981-95 mean minus the 1961-75 mean). The solid and dashed denote the decadal differences derived from the Levitus data, the SODA data, respectively. The dotted line denotes the corresponding decadal difference in thermocline depth obtained from the CZ ocean model forced by the FSU wind.

Fig. 3 Decadal differences in the mean depth of the 20°C isotherm (the 1981-95 mean minus the 1961-75 mean). The solid and dashed denote the decadal differences derived from the Levitus data, the SODA data, respectively. The dotted line denotes the corresponding decadal difference in thermocline depth obtained from the CZ ocean model forced by the FSU wind.

Fig. 4 Time longitude section of the SST anomalies averaged over 5ºS-5ºN and the power spectra of time series of Niño-3 SST anomalies (°C) (5ºS-5ºN, 150ºW-90ºW) in log units obtained from the CZ model benchmark experiments with (a) the 1961-75 and (b) the 1981-95 basic state.

Fig. 4 Time longitude section of the SST anomalies averaged over 5ºS-5ºN and the power spectra of time series of Niño-3 SST anomalies (°C) (5ºS-5ºN, 150ºW-90ºW) in log units obtained from the CZ model benchmark experiments with (a) the 1961-75 and (b) the 1981-95 basic state.

Fig. 5 The same as in Fig. 1 except that the results are derived from the CZ model outputs using the 1961-75 (left panel) and 1981-95 (right panel) basic state. First JSVD modes for the period of 1961-75 and 1981-95 explain 97.2% and 97.9% of total variance, respectively

Fig. 5 The same as in Fig. 1 except that the results are derived from the CZ model outputs using the 1961-75 (left panel) and 1981-95 (right panel) basic state. First JSVD modes for the period of 1961-75 and 1981-95 explain 97.2% and 97.9% of total variance, respectively

WANG AND AN: WHY THE EL NINO CHANGED DURING THE LATE 1970S
WANG AND AN: WHY THE EL NINO CHANGED DURING THE LATE 1970S
WANG AND AN: WHY THE EL NINO CHANGED DURING THE LATE 1970S

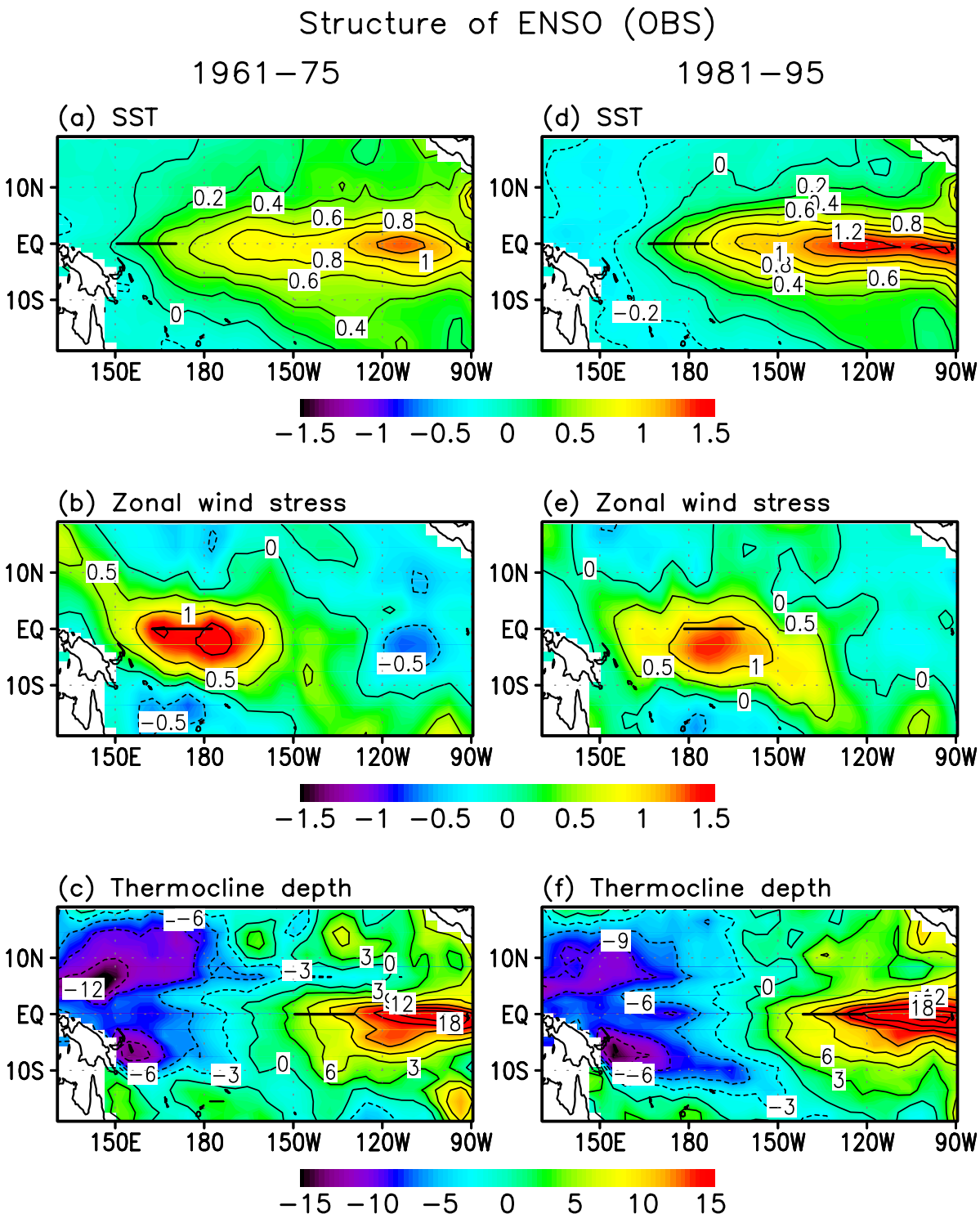
Structure of ENSO (OBS)
1961−75
1981−95
(a) SST
(d) SST
(b) Zonal wind stress
(e) Zonal wind stress
(c) Thermocline depth
(f) Thermocline depth
10N
EQ
10S
150E
180
150W
120W
90W
−1.5 −1 −0.5 0 0.5 1 1.5
−15 −10 −5 0 5 10 15

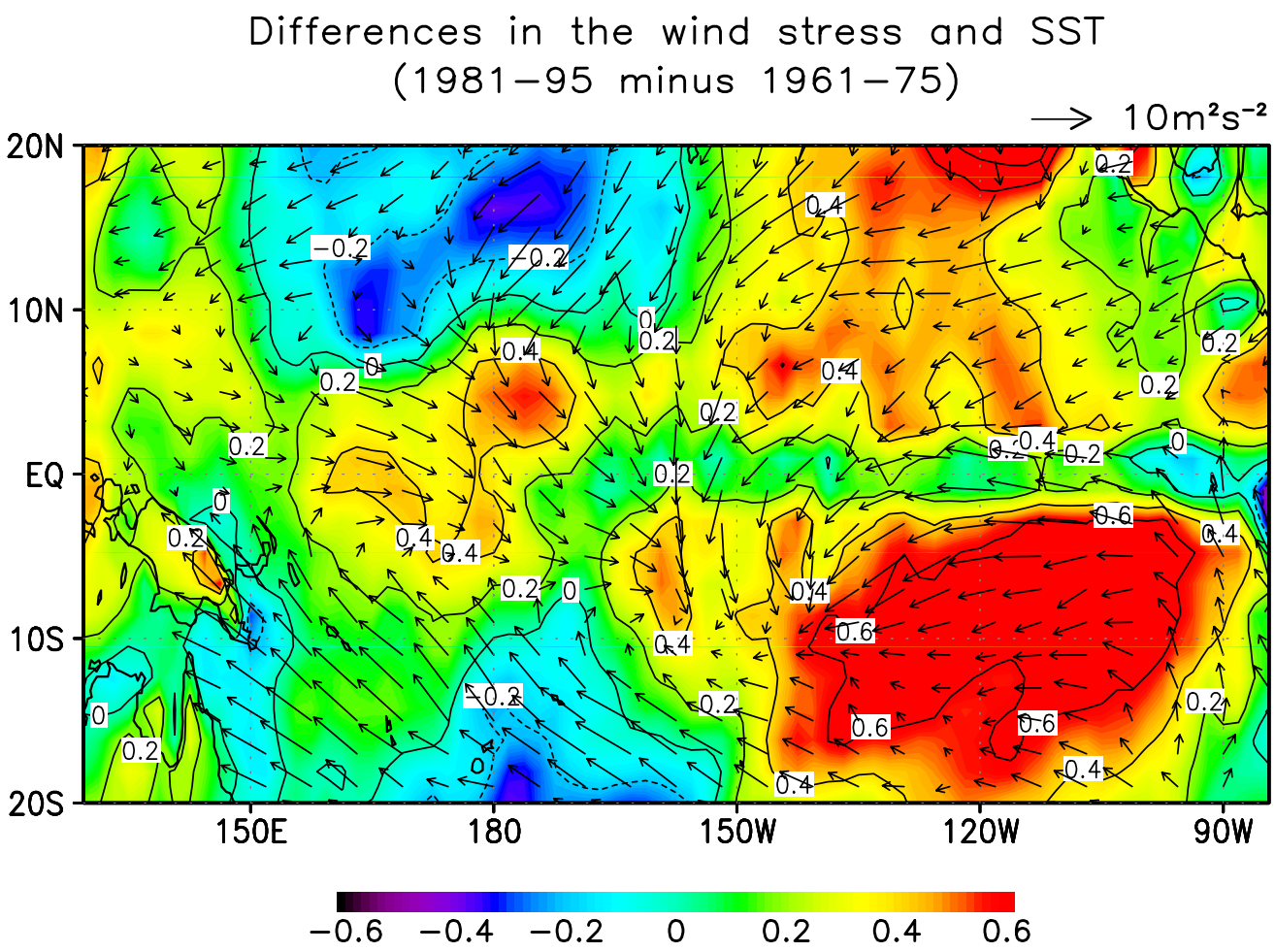
Differences in the wind stress and SST
(1981–95 minus 1961–75)
10m²s⁻²
20N
10N
EQ
10S
20S
150E
180
150W
120W
90W
−0.6
−0.4
−0.2
0
0.2
0.4
0.6

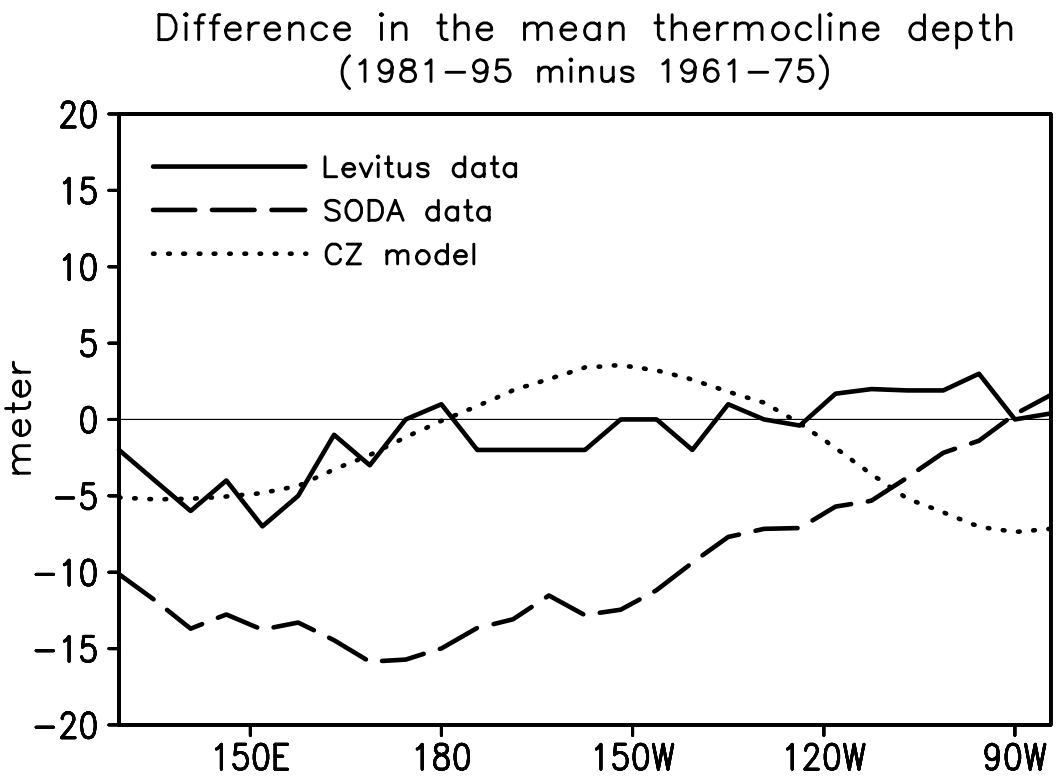
Difference in the mean thermocline depth
(1981–95 minus 1961–75)
Levitus data
SODA data
CZ model
meter
20
15
10
5
0
−5
−10
−15
−20
150E
180
150W
120W
90W

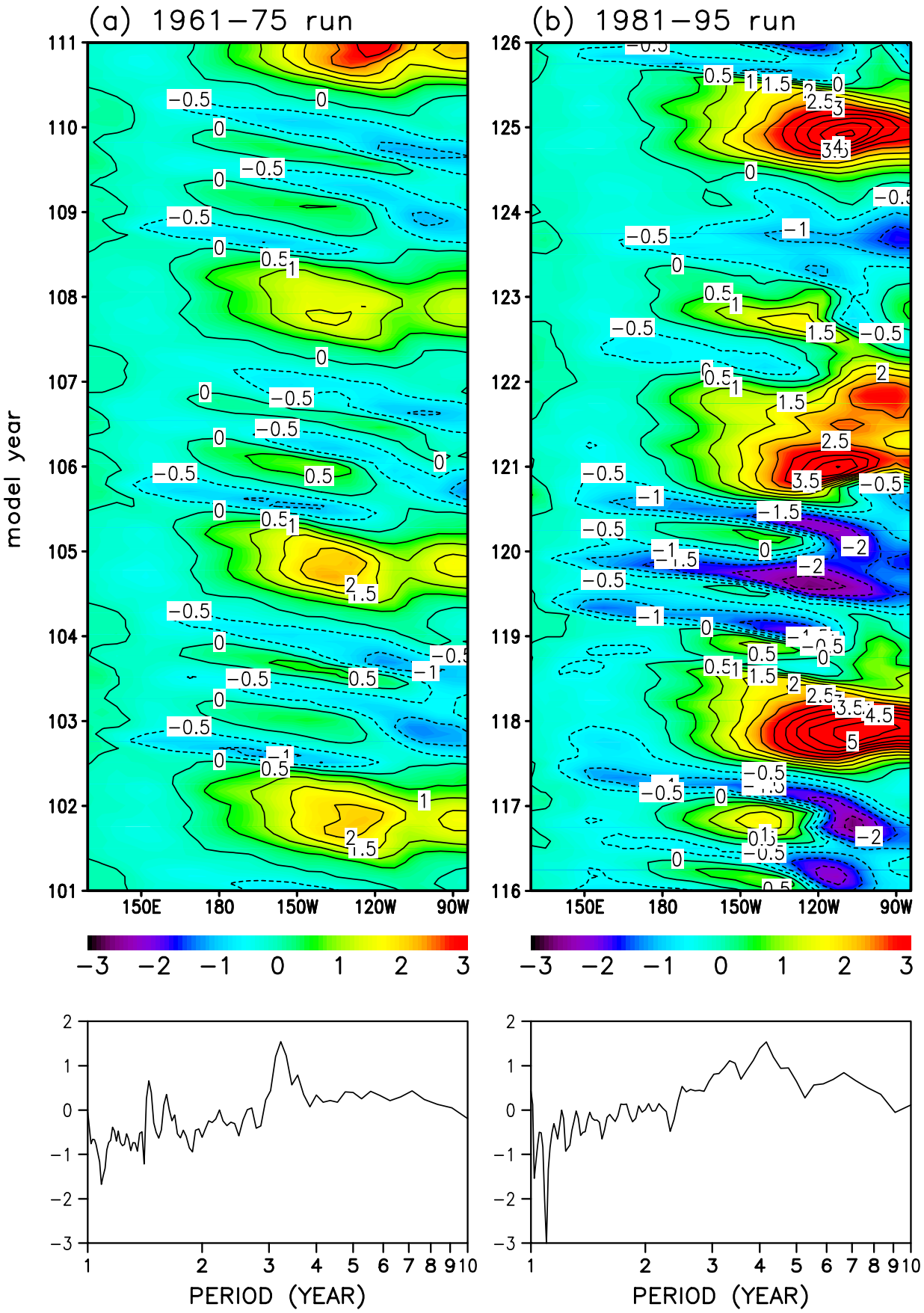
(a) 1961−75 run
(b) 1981−95 run
model year
150E
180
150W
120W
90W
−3 −2 −1 0 1 2 3
PERIOD (YEAR)

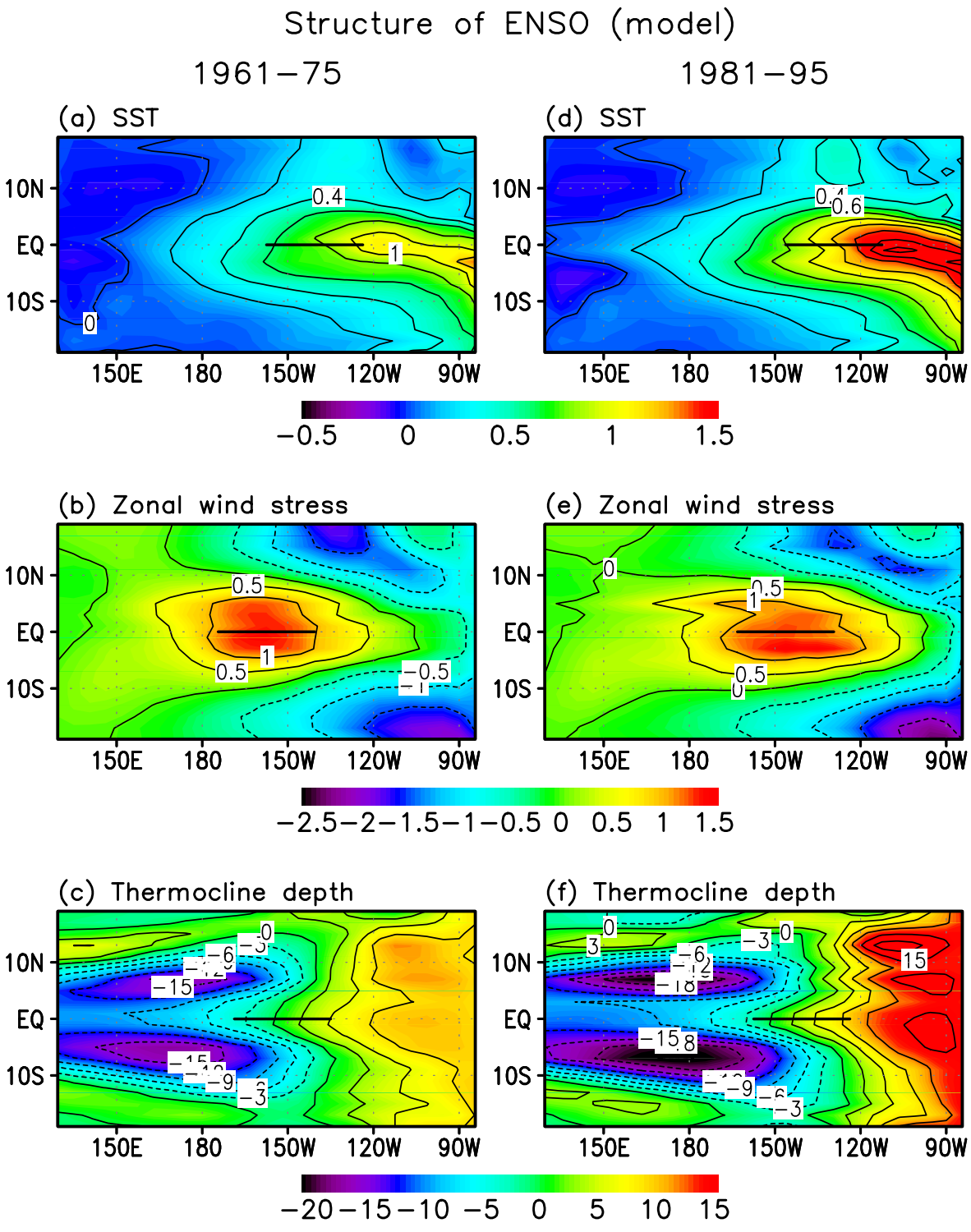
Structure of ENSO (model)
1961–75
1981–95
(a) SST
(d) SST
10N
EQ
10S
150E
180
150W
120W
90W
0.4
1
0
0.6
−0.5
0
0.5
1
1.5
(b) Zonal wind stress
(e) Zonal wind stress
0.5
1
−0.5
0
−2.5
−2
−1.5
−1
(c) Thermocline depth
(f) Thermocline depth
−15
−9
−3
3
15
−20
−15
−10
−5
5
10